Fast Atom Diffraction from Superstructures on a Fe(110) Surface

A. Schüller, M. Busch, S. Wethekam, and H. Winter*

Institut für Physik, Humboldt Universität zu Berlin, Brook-Taylor-Strasse 6, D-12489 Berlin-Adlershof, Germany

(Received 2 September 2008; published 8 January 2009)

Fast atoms with energies from 500 eV up to several keV are grazingly scattered from a Fe(110) surface covered with defined superstructures of sulfur or oxygen atoms. For scattering along low index azimuthal directions, we observe defined diffraction patterns in the angular distributions for scattered projectiles. From the analysis of those patterns, we derive the widths of low indexed axial channels and the corrugation of the interaction potential across these channels. This allows us to estimate the positions of adsorbed atoms on the Fe(110) surface. By demonstration, for adsorbate induced superstructures on a metal surface, we show that fast atom diffraction, first observed for insulators, can be applied to studies on surface structures for a wide range of materials.

DOI: 10.1103/PhysRevLett.102.017602 PACS numbers: 79.20.Rf, 34.20.Cf, 68.49.Bc, 79.60.Bm

Recently, quantum diffraction effects have been demonstrated for grazing scattering of fast atoms with energies ranging from some 100 eV to about 10 keV from monocrystalline insulator surfaces [1–3]. The presence of diffraction patterns in the intensity distributions after scattering of fast atoms can be understood by specific features for grazing collisions with a crystal surface. In the regime of ''surface channeling'' [4,5], a high angular resolution can be obtained for polar incidence angles Φ_{in} of typically 1 deg. Then, diffraction for scattering from atomic strings separated by a distance d can be observed for atoms of mass M and velocity v even for de Broglie wavelengths $\lambda_{dB} = h/Mv \ll d$, since small diffraction angles Ψ, resulting from the Bragg condition $n\lambda_{dB} = d\sin\Psi$ for diffraction orders n, can be resolved. Furthermore, the corrugation of the interaction potential between strings of surface atoms results in a *blazing effect* so that—similar as for a diffraction grating—the flux of particles is directed into higher diffraction orders.

In this Letter, we demonstrate that the phenomenon of Fast Atom Diffraction (FAD) under axial surface channeling conditions is not restricted to scattering from clean and ordered insulator surfaces. We have observed defined diffraction patterns also for scattering of fast atoms from a Fe(110) surface covered with two different superstructures formed by sulfur or oxygen atoms. Owing to metal-like properties of such adsorbate-metal systems with significantly enhanced electronic excitation probabilities, the feasibility of FAD was an open question so far. The strong interactions of projectiles with metal surfaces via electronic excitations will result in considerable contributions of decoherence so that diffraction may not be observed. Here, we demonstrate that this is not the case. As a first application of the new method, we show that detailed structural information on the adsorbates at the topmost surface layer can be derived.

In our experiments, we have scattered neutral H_2 molecules, ^{3}He and ^{4}He atoms with energies E_0 ranging from 0.4 keV up to 3 keV from a clean and adsorbate covered Fe(110) surface under grazing angles of incidence $\Phi_{in} \leq 1.5$ deg. Fast neutral beams were produced via neutralization of ions in a gas cell mounted in front of a UHV chamber (base pressure some 10^{-11} mbar). The Fe(110) target surface was prepared by cycles of grazing sputtering with 25 keV Ar^+ ions and subsequent annealing to about 500 °C. Superstructures with sulfur atoms were produced in several cycles of annealing at 730 °C by segregation from bulk impurities of the crystal [6], superstructures with oxygen atoms by adsorption of O_2 for a dose of 2 L (1 L = 1 Langmuir = 1.33×10^{-6} mbar s) at a pressure of 5×10^{-9} mbar, and subsequent annealing at 500 °C for 10 minutes [7]. Using a SPALEED instrument (Omicron Nanotechnology GmbH), we observed sharp spots for $c(1 \times 3)$S/Fe(110) [8,9] and $c(2 \times 2)$O/Fe(110) [7,10,11]. The scattering experiments were performed in the regime of axial surface channeling [4,5]; i.e., low indexed directions in the surface plane of the target were adjusted along the incident projectile beam. Two dimensional angular distributions of scattered projectiles were recorded 66 cm behind the target with a position sensitive microchannel plate [12]. This provides an efficient recording of data, where complete diffraction patterns can be recorded in a time of several seconds up to some minutes. Since only about 10^4 light atoms per second hit the target surface, the method is nondestructive and can be applied for studies on insulator surfaces [1–3] and, as demonstrated here, on adsorption phenomena at metal surfaces, too. This holds especially for sensitive surface structures which can be modified or even destroyed by conventional techniques as, for, e.g., LEED [13].

In Fig. 1, we display 2D intensity distributions for 0.6 keV ^{3}He atoms scattered from a clean Fe(110) surface (upper panel), from $c(1 \times 3)$S/Fe(110) (middle panel), and from $c(2 \times 2)$O/Fe(110) (lower panel) along a $\langle 1\bar{1}1 \rangle$ direction. Whereas for the clean surface we find a dominant single spot and a marginal indication for first order diffraction spots only, we observe for scattering from the surface with ordered superstructures intensity patterns with a num-

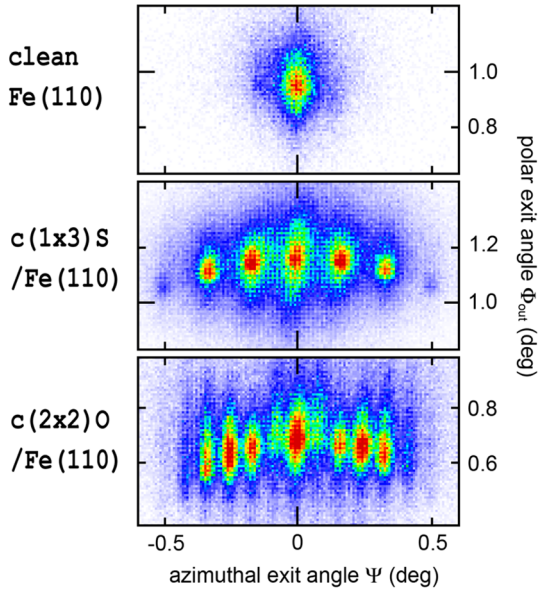

FIG. 1 (color online). Two dimensional intensity distributions as recorded with microchannel plate detector for scattering of 0.6 keV ^{3}He atoms along $\langle 1\bar{1}1\rangle$ direction from clean Fe(110) under $\Phi_{in} = 0.98$ deg (upper panel), from $c(1 \times 3)$S/Fe(110) under $\Phi_{in} = 1.17$ deg (middle panel) and from $c(2 \times 2)$O/Fe(110) under $\Phi_{in} = 0.71$ deg (lower panel). Color code: red/gray = high intensity, blue/black = low intensity.

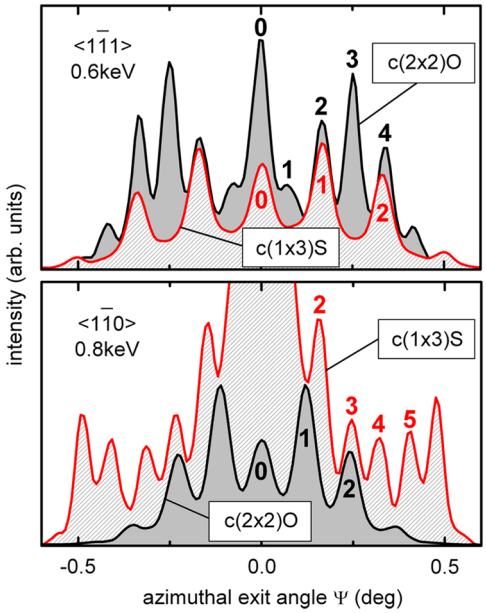

FIG. 2 (color online). Projection of intensity distributions on azimuthal exit angle Ψ for scattering of 0.6 keV ^{3}He atoms along $\langle 1\bar{1}1\rangle$ direction (upper panel) and 0.8 keV ^{3}He atoms along $\langle 1\bar{1}0\rangle$ direction (lower panel) from $c(2 \times 2)$O/Fe(110) (black curves) and $c(1 \times 3)$S/Fe(110) (red/gray curves).

ber of diffraction spots. For axial surface channeling follows from the Bragg condition for the interval of the azimuthal angle of adjacent diffraction spots $\Delta\Psi \simeq \lambda_{dB}/d$ which is independent of the angle of incidence Φ_{in}. However, for deflection of projectiles into diffraction orders $n > 0$, a sufficient corrugation is necessary. The angular distributions in Fig. 1 imply an increased corrugation across $\langle 1\bar{1}1\rangle$ channels for $c(1 \times 3)$S/Fe(110) and $c(2 \times 2)$O/Fe(110) compared to clean Fe(110). The enhancement of the corrugation is an important property for structural studies.

In the upper panel of Fig. 2, we show the projection of the intensity distributions of the middle and lower panels of Fig. 1 on the azimuthal exit angle Ψ. For scattering from $c(2 \times 2)$O/Fe(110) (black curve), the azimuthal distance $\Delta\Psi$ of adjacent diffraction peaks is half the distance for $c(1 \times 3)$S/Fe(110) (red/gray curve). In the lower panel of Fig. 2, we show the projection of intensity distributions on the azimuthal exit angle for scattering of 0.8 keV ^{3}He atoms incident along a $\langle 1\bar{1}0\rangle$ direction. Here, in contrast to the $\langle 1\bar{1}1\rangle$ directions (upper panel of Fig. 2), $\Delta\Psi$ for $c(2 \times 2)$O/Fe(110) (black curve) is larger than for $c(1 \times 3)$S/Fe(110) (red/gray curve) by a factor of 1.5. These factors are in accord with the relative widths of the corresponding axial channels (see discussion below).

For illustration, we show in Fig. 3 a sketch of a top view of structural models for $c(1 \times 3)$S/Fe(110) (left panel) [8,9] and $c(2 \times 2)$O/Fe(110) (right panel) [10]. The axial channels of both superstructures have fairly different widths. For, e.g., the $c(1 \times 3)$S/Fe(110) structure one finds a broad channel along $\langle 1\bar{1}0\rangle$ and a fairly narrow one along $\langle 1\bar{1}1\rangle$, whereas the opposite holds for the $c(2 \times 2)$O/Fe(110) structure. The channel widths can directly be deduced from the diffraction patterns.

The diffraction spots in Fig. 1 result from the periodicity of the corrugated interaction potential reflecting the geometrical arrangement of surface atoms forming axial channels of width d in the topmost surface layer [1–3]. For small azimuthal scattering angles Ψ in the surface plane, positions of diffraction spots follow from the Bragg condition $n\lambda_{dB} = d \sin\Psi$ with splittings between adjacent diffraction spots $\Delta\Psi \simeq \lambda_{dB}/d$. In Fig. 4, we have plotted $\Delta\Psi$ as a function of the de Broglie wavelength λ_{dB} for

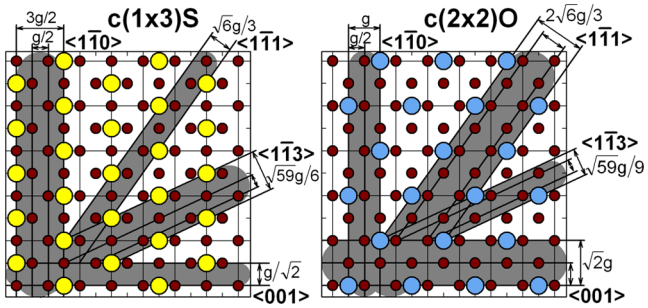

FIG. 3 (color online). Sketch of top view of structural models for $c(1 \times 3)$S/Fe(110) (left panel) and $c(2 \times 2)$O/Fe(110) (right panel). Some low indexed axial channels are highlighted. Widths d of channels are given with respect to Fe lattice constant $g = 2.86$ Å (see also Table I). Fe atoms of first (110) layer: small red circles, S atoms (left panel): large yellow circles and O atoms (right panel): large blue circles.

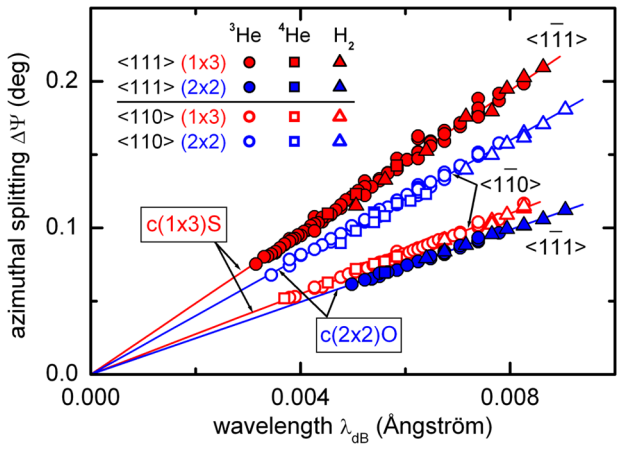

FIG. 4 (color online). Azimuthal angular splitting $\Delta\Psi$ of diffraction spots as function of de Broglie wavelength λ_{dB} for scattering of H_2 molecules, ^{3}He and ^{4}He atoms from $c(1 \times 3)$S/Fe(110) (red/gray symbols) and $c(2 \times 2)$O/Fe(110) (blue/black symbols) along $\langle 1\bar{1}0\rangle$ (open symbols) and $\langle 1\bar{1}1\rangle$ (full symbols). Red/gray and blue/black lines: best linear fits to data.

grazing scattering of H_2 molecules, ^{3}He and ^{4}He atoms from $c(1 \times 3)$S/Fe(110) and $c(2 \times 2)$O/Fe(110) along $\langle 1\bar{1}0\rangle$ and $\langle 1\bar{1}1\rangle$. We reveal the expected linear dependence on λ_{dB} with slope $1/d$ and different d at same channeling direction for the two superstructures.

In Table I, we list the channel widths d derived from best linear fits to data as shown in Fig. 4 for four low index channels of the two superstructures. Within the accuracy for the deduced widths d (limited to some percent owing to uncertainties in angle and projectile energy), their values scale well in integer multiples of theoretical widths for the unreconstructed Fe(110) substrate [14] (third row of Table I).

The relative intensities for diffraction spots of different order n (cf. Fig. 2) are determined by the corrugation of the interaction potential [1,2]. Recently, we pointed out that the concept of *supernumerary rainbows* [15] is applicable here [3]. Thus, from an analysis of spot intensities, one can derive the corrugation which yields information on the vertical positions of adsorbed atoms. We demonstrate this feature for the intensities of the diffraction spots recorded for scattering of ^{3}He atoms from $c(2 \times 2)$O/Fe(110) along $\langle 1\bar{1}0\rangle$.

For *axial channeling*, projectile trajectories result from steering by a large number of atoms along strings in terms of small angle scattering. The scattering potential is well approximated by an averaging of pair potentials along atomic strings in terms of a continuum potential which depends on the distance from a string only [4]. Then, the motion of projectiles parallel to strings proceeds with constant kinetic energy and is separated from the motion in a plane normal to atomic strings (surface plane) with energy $E_\perp = E_0 \sin^2\Phi_{in}$. In a semiclassical theory for scattering from a sinusoidal hard wall [16], the intensity of a diffraction spot of order n is given by $J_n^2\{\frac{\Delta z}{2} k_\perp[1 + \sqrt{1 - (\frac{2\pi n}{k_\perp d})^2}]\}$ with J_n being the Bessel function of order n, $k_\perp$ the wave number ascribed to the normal motion of atoms with energy $E_\perp = \hbar^2 k_\perp^2/2M$, and Δz the full corrugation of the interaction potential across the axial channel. We use $J_n^2(\Delta z k_\perp)$ as a good approximation for $n = 0$ and 1 for the present case.

In Fig. 5 (upper panel), we show the relative spot intensities for the diffraction orders $n = 0$ (blue/black circles) and $n = 1$ (red/gray squares) as function of the wave number $k_\perp$ for scattering of ^{3}He atoms from $c(2 \times 2)$O/Fe(110). The solid curves (blue/black and red/gray) represent best fits to $J_n^2(\Delta z k_\perp)$, where the fit parameter Δz is assumed to dependent linearly on the normal energy $E_\perp$. Decoherence effects ascribed to electronic excitations of the target with increasing $k_\perp(E_\perp)$ are taken into account by an exponential damping of the oscillation amplitudes. We note that this damping term has a minor influence on the positions of the extrema in the fits and, hence, on Δz. With these Δz, calculated intensities for diffraction spots of orders $n > 1$ are also in good agreement with our experiments. In order to relate the corrugation across the channel to the positions of O atoms at a distance h above the surface, we calculated the interaction potentials averaged along atomic strings from interatomic pair potentials based on Thomas-Fermi screening [17]. We note that we obtained for this potential good agreement with respect to the rainbow angles for classical scattering [18,19] at projectile energies of several keV.

The thin solid curves in the lower panel of Fig. 5 represent the full corrugation Δz calculated for different normal positions h for O atoms at fourfold hollow sites. Best agreement with the experiment is achieved for h slightly above 1.1 Å. We apply the same procedure for scattering along $\langle 1\bar{1}3\rangle$. For this direction, h is also close to 1.1 Å. This value for h is in good accord with recent DFT calculations for the system $c(2 \times 2)$O/Fe(110), where for an oxygen coverage of 50% of a monolayer $h = 1.03$ Å [10] and $h = 1.11$ Å [11] is reported. Although the determination of the

TABLE I. Widths d of axial channels along $\langle 1\bar{1}1\rangle$, $\langle 1\bar{1}0\rangle$, $\langle 1\bar{1}3\rangle$, and $\langle 001\rangle$ directions in Ångström for $c(1 \times 3)$S/Fe(110) and $c(2 \times 2)$O/Fe(110) deduced from the present experiments and for Fe(110) (with Fe lattice constant $g = 2.86$ Å).

	$\langle 1\bar{1}1\rangle$	$\langle 1\bar{1}0\rangle$	$\langle 1\bar{1}3\rangle$	$\langle 001\rangle$
$c(1 \times 3)$S/Fe(110)	2.36	4.17	3.56	2.02
$c(2 \times 2)$O/Fe(110)	4.64	2.87	2.48	4.03
Fe(110)	$\sqrt{6}g/3 = 2.34$	$g/2 = 1.43$	$\sqrt{59}g/18 = 1.22$	$g/\sqrt{2} = 2.02$

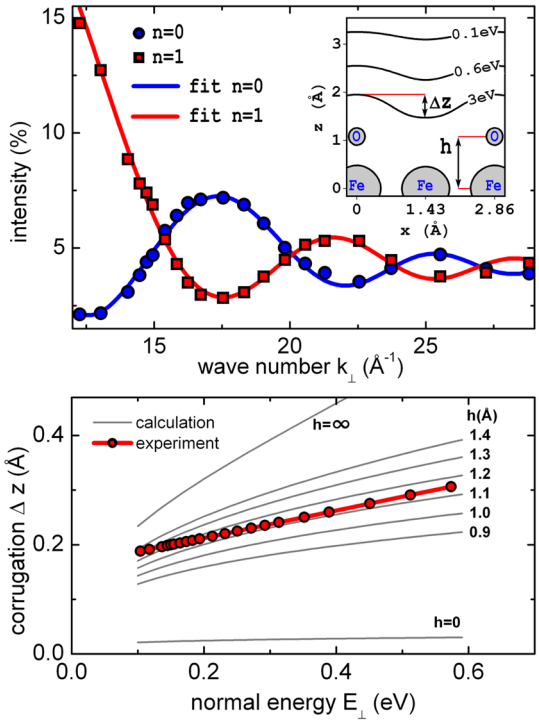

FIG. 5 (color online). Upper panel: Relative intensity of zeroth order (blue/black circles) and first order (red/gray squares) diffraction spots as function of wave number $k_\perp$ for scattering of ^{3}He atoms from $c(2\times 2)$O/Fe(110) along $\langle 1\bar{1}0\rangle$. Curves represent best fits of Bessel functions $J_n^2(\Delta z k_\perp)$ to data as detailed in text. Inset: sketch of arrangement of atoms normal to $\langle 1\bar{1}0\rangle$ and equipotential lines for normal energies $E_\perp = 0.1$, 0.6, and 3 eV. Lower panel: Full corrugation Δz as function of normal energy $E_\perp$. Red/gray circles: result from best fit; thin solid curves: calculations with interaction potential from Ref. [18] for different h.

corrugation using interference of fast atoms has a high intrinsic accuracy, we have to stress that the interaction potential in this collision regime and the hard wall approximation used in the analysis of data restricts our estimate on the position h of the oxygen atoms to about 0.3 Å.

In conclusion, we have observed diffraction patterns for axial surface channeling of fast neutral H_2 molecules, ^{3}He and ^{4}He atoms from a Fe(110) surface covered by $c(2\times 2)$ and $c(1\times 3)$ superstructures formed by O and S atoms, respectively. From the evaluation of the diffraction pattern for a number of low indexed axial channels, we deduced their widths and for $c(2\times 2)$O/Fe(110) the corrugation of the interaction potential across the $\langle 1\bar{1}0\rangle$ channel. Furthermore, from the corrugation of the potential derived from intensity modulations of diffraction spots, we estimated the transverse positions of O atoms in accord with recent DFT calculations [10,11]. Similar diffraction effects are also observed for more complex superstructures. This points to a powerful alternative method in the analysis of surface structures, which combines the benefits of techniques related to real space and diffraction. First, prominent axial channels are identified and basic structural information is provided (those studies can be extended at higher projectile energies to classical rainbow scattering). Second, the diffraction patterns yield information on the widths of the axial channels, and, third, from the intensity variation of diffraction spots, the corrugation of the potential for specific axial channel and the transverse positions of adatoms can be obtained. In previous work, Fast Atom Diffraction (FAD) has been observed only for surfaces with an electronic band gap, where electronic excitations are strongly suppressed. Our study on adsorbate induced superstructures on a metal surface shows that FAD can be applied to wide range of materials in order to deduce detailed information on atomic arrangements at solid surfaces.

We thank the DFG (Project Wi 1336) for financial support and K. Maass, G. Lindenberg, and U. Linke (FZ Jülich) for their assistance in the preparation of the experiments.

*Author to whom correspondence should be addressed. winter@physik.hu-berlin.de

[1] A. Schüller, S. Wethekam, and H. Winter, Phys. Rev. Lett. **98**, 016103 (2007).
[2] P. Rousseau, H. Khemliche, A. G. Borisov, and P. Roncin, Phys. Rev. Lett. **98**, 016104 (2007).
[3] A. Schüller and H. Winter, Phys. Rev. Lett. **100**, 097602 (2008).
[4] D. Gemmell, Rev. Mod. Phys. **46**, 129 (1974).
[5] H. Winter, Phys. Rep. **367**, 387 (2002).
[6] J. Weissenrieder, M. Göthelid, G. Le Lay, and U. O. Karlsson, Surf. Sci. **515**, 135 (2002).
[7] M. Busch, M. Gruyters, and H. Winter, Surf. Sci. **600**, 4598 (2006).
[8] L. Berbil-Bautista, S. Krause, T. Hänke, M. Bode, and R. Wiesendanger, Surf. Sci. **600**, L20 (2006).
[9] M. J. S. Spencer, I. K. Snook, and I. Yarovsky, J. Phys. Chem. B **110**, 956 (2006).
[10] P. Błoński, A. Kiejna, and J. Hafner, Surf. Sci. **590**, 88 (2005).
[11] P. Błoński, A. Kiejna, and J. Hafner, Phys. Rev. B **77**, 155424 (2008).
[12] Roentdek GmbH, Kelkheim-Ruppertshain, Germany.
[13] J. P. Toennies, F. Traeger, J. Vogt, and H. Weiss, J. Chem. Phys. **120**, 11347 (2004).
[14] C. Leygraf and S. Ekelund, Surf. Sci. **40**, 609 (1973).
[15] W. F. Avrin and R. P. Merrill, Surf. Sci. **311**, 269 (1994).
[16] R. I. Masel and R. P. Merrill, J. Chem. Phys. **65**, 2690 (1976).
[17] D. J. O'Connor and J. Biersack, Nucl. Instrum. Methods Phys. Res., Sect. B **15**, 14 (1986).
[18] A. W. Kleyn and T. C. M. Horn, Phys. Rep. **199**, 191 (1991).
[19] A. Schüller, G. Adamov, S. Wethekam, K. Maass, A. Mertens, and H. Winter, Phys. Rev. A **69**, 050901(R) (2004).